small structures
www.small-structures.com

Electrons, Localization but no Hopping: Disorder as Key for Understanding Charge Transport in Mesoporous Silicon

Tommy Hofmann, Haider Haseeb, Danny Kojda, Natalia Gostkowska-Lekner, and Klaus Habicht*

This article presents a unique study on the charge carrier transport in electrochemically anodized mesoporous silicon by combining macroscopic conductivity and thermopower measurements. Temperature-dependent electrical conductivity measurements reveal a thermally activated transport in extended electronic states. An intrinsic variation of the thermal activation energies from sample to sample upon apparent identical synthesis conditions is discussed in terms of microscopic disorder. In a detailed analysis of the activation energies, the existence of a disorder-dependent mobility edge between localized and extended states in a band tail with exponential density-of-states becomes indispensable for understanding the microscopic transport mechanism. The observation of a Meyer–Neldel compensation rule for the conductivity between different samples is a direct consequence of this mobility edge. Temperature-dependent thermopower measurements provide further, stringent proof for disorder-dominated transport in extended states above the mobility edge and dispel an alternative explanation attempt for the Meyer–Neldel rule in mesoporous silicon based on multiphonon absorption upon charge carrier transport.

1. Introduction

In recent years, the emergence of novel nanostructured materials has attracted significant attention from researchers, who have recognized their huge potential to drive advancements in fundamental research as well as in applied science and engineering. The advent of a range of sophisticated techniques to precisely control material design at the nanoscale has enabled the synthesis of a vast array of materials, including nanowires,[1–4] nanodots,[5,6] nanosculptured interfaces,[7,8] thin films,[9–11] and complex heterostructures.[12–16]

Nanostructuring materials raises a number of important scientific questions of immediate relevance to their functional properties. How do material properties alter when systems transit from macroscopic to nanoscopic length scales? How do reduced dimensionality, interface effects, and even quantum effects influence static and dynamic material behavior? What are the effects of nanoscale confinement on soft[17] and hard matter?

Elastic X-ray and neutron scattering studies have demonstrated that nanoconfinement induces modified structural phase transitions in both hard and soft matter.[18,19] Impedance spectroscopy has revealed that electronic properties in nanometer-sized dielectrics substantially differ from those of bulk systems.[20] Nanostructuring introduces scattering centers for phonons or even modifies the phonon dispersion, thus affecting thermal transport.[21–28] The complex geometry of porous networks, combined with liquid-interface interactions, determines the hydrodynamic flow in nanochannels.[29] At a smaller length scale, the stochastic motions of molecules in liquids are constrained by geometrical restrictions.[30,31]

These insights provide motivation for scientists to engage in the search for novel nanosized material classes and their potential technological applications. Nanostructured systems, for instance, are envisioned as the next generation of energy materials that would allow the implementation of a sustainable, affordable, and green energy infrastructure.[32]

Ionic liquids embedded in porous carbons are promising candidates for supercapacitors with enhanced power densities. Nanostructured silicon or nanoconfined sulfur are discussed as electrodes for novel batteries fueling the hope to extend cycle robustness and thus battery lifetime. Nanostructured electron–donor/electron–acceptor systems represent a promising pathway toward high-efficiency polymer-based photovoltaics. The present study focuses on mesoporous silicon which is drawing remarkable interest for heat management in future information

T. Hofmann, H. Haseeb, D. Kojda, N. Gostkowska-Lekner, K. Habicht
Department Dynamics and Transport in Quantum Materials
Helmholtz-Zentrum Berlin für Materialien und Energie GmbH
Hahn-Meitner-Platz 1, 14109 Berlin, Germany
E-mail: tommy.hofmann@helmholtz-berlin.de

H. Haseeb, N. Gostkowska-Lekner, K. Habicht
Institut für Physik und Astronomie
Universität Potsdam
Karl-Liebknecht-Straße 24/25, 14476 Potsdam, Germany

The ORCID identification number(s) for the author(s) of this article can be found under https://doi.org/10.1002/sstr.202400437.

DOI: 10.1002/sstr.202400437

technologies and thermoelectrics for thermal to electric power conversion.

Mesoporous silicon—hereafter referred to as pSi—is defined as single-crystalline silicon penetrated by nanometer-sized pores. Its synthesis by electrochemical anodization in hydrofluoric (HF) acid is moderately complex,[33,34] but offers benefits such as scalability together with a high degree of tunability. The parameters of the anodization process allow for the control of porosity, pore size distribution, pore connectivity, and pore orientation.[35]

PSi has a multitude of potential applications. Its biocompatibility makes it an attractive material for biosensors and drug delivery.[36,37] Filters and nanofluidics seek to benefit from the flow dynamics of gases and liquids in the pore network. The huge internal surfaces inherent to the material are interesting for battery anodes[38] and capacitors,[39] while thermoelectric applications exploit the material's exceptionally low thermal conductivity.[40]

Some of the envisioned applications rely on the geometric confinement provided by the material, its huge surfaces, or the host–guest interaction. Others depend more directly on the intrinsic properties of the material, such as thermal conductivity and electric conductivity. In the latter case, a fundamental understanding of transport phenomena in the material is indispensable. A thorough understanding of phonon and charge transport is a prerequisite for any successful and well-conceived material design strategy.

Surprisingly, despite the widespread attention awarded to pSi, there is still no coherent picture describing the charge carrier transport mechanism in the pSi skeleton. This study presents temperature-dependent electrical conductivity and thermopower measurements on an ensemble of different pSi samples. A detailed data analysis unambiguously identifies the underlying process that defines the electronic transport properties of the material to be governed by extended states above a disorder-dependent mobility edge rather than multiphonon-assisted hopping between localized states.

2. Results and Discussion

Although mesoporous silicon is synthesized from highly conductive boron-doped wafers, it does, however, not inherit the conductivity $\sigma = 50 - 100\,\mathrm{S\,cm^{-1}}$ of the source material. In fact, the anodization process reduces σ by up to seven orders of magnitude at $T = 300\mathrm{K}$ (**Figure 1**).

The conductivity of the p-doped Si wafers exhibits a temperature dependence typical of highly doped semiconductors (Figure 1 inset),[41] where the hole mobility is reduced at higher temperatures due to increased electron–phonon scattering rates. As a consequence, $\sigma(T)$ decreases in the intrinsic region ($T > 100\mathrm{K}$) with increasing temperature.[41] In contrast, pSi membranes ($W \times H \times D \approx 3 \times 0.2 \times 10\,\mathrm{mm^3}$) show thermally activated charge transport (Figure 1) in the probed temperature range $T > 300\mathrm{K}$.

Addressing charge carrier scattering and modified band structure in pSi precedes necessarily the discussion of the conductivity and the microscopic transport mechanism. It is obvious that pSi as disordered, defective structure introduces additional scattering centers for "freely" moving electrons. These scattering

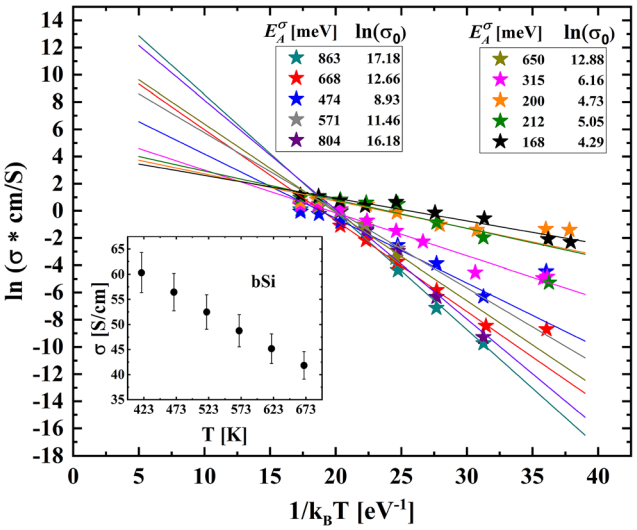

Figure 1. Temperature-dependent electrical conductivity of various pSi samples. The solid lines represent nonlinear least squares approximations to the datasets based on Equation (1). The two data columns are the optimized model parameters. Error bars are of a similar size than the symbols. The inset shows the *T*-dependent conductivity of the source material, p-doped bulk silicon.

centers impair carrier transport as the additional scattering length defined by the nanometer-sized pore–pore distance is at least comparable or even smaller than the one in the source material bulk silicon (bSi). The modified scattering rates are important for transport in extended states whereas hopping in localized states is governed by tunneling rates.[42]

Subtle and diverse effects lead to modifications of the band structure in pSi. The electronic band structure of pSi differs significantly from the one of crystalline bSi. The broken translational symmetry at the pore interfaces gives rise to midgap states. These states are responsible for band bending and depletion of free charge carriers in the only several nanometer thick Si walls.[41] The spatial confinement of carriers in a crystalline Si skeleton with nanometer thick walls increases the bandgap in pSi to 1.46eV for all samples compared to an optical gap of 1.14eV at 300K in bSi. This confinement-induced change in band structure is most evident in UV–vis spectra (**Figure 2**) where the absorption threshold in pSi is redshifted.

Random disorder in pSi causes Anderson localization.[43] These localized states act as additional carrier traps and create exponential band tails in the density-of-states. The prominent Urbach tails in the absorbance α (Figure 2) reflect these band tails with exponential density-of-states.[44]

From the prelude it becomes evident that the one key question at the forefront of the discussion is, whether carrier transport happens in extended states or in localized states via hopping. In the case of hopping transport, the quest to identify a particular hopping mechanism such as single phonon-assisted hopping,[42,45] or multiphonon-assisted, polaronic hopping,[46] complements this key question.

The conductivity measurements in Figure 1 help providing answers systematically. The data show thermally activated transport according to

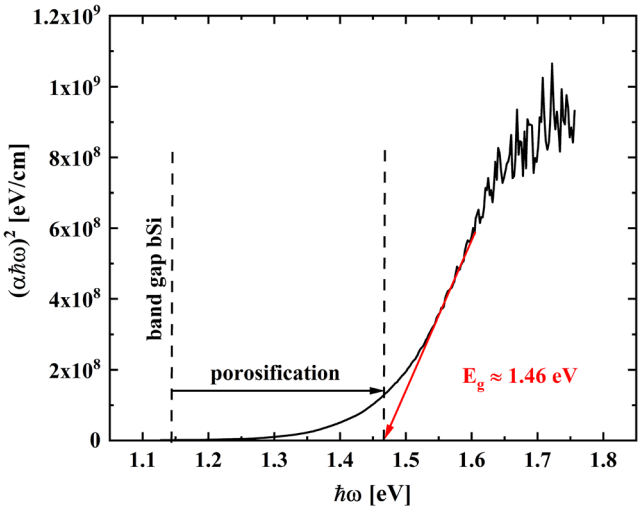

Figure 2. Optical bandgap in pSi at $T = 300$K : the Tauc plot exhibits the dependence of the absorbance α on the incident photon energy $\hbar\omega$.[74,75] Optical bandgap of pSi 1.46eV and bulk silicon 1.14eV are marked.

$$\sigma(T) = \sigma_0 \exp\left(-E_A^\sigma \Big/ k_B T\right) \tag{1}$$

where E_A^σ refers to the activation energy of the transport process. The temperature dependence of the parameter σ_0, which usually takes some form of a power law[41,42] for ordered and disorder semiconductors, is negligible compared to the dominant exponential term.

Activation energies E_A^σ vary from sample to sample. The lower threshold is around 170meV . The upper threshold of 860meV is close to half the size of the optical bandgap in pSi. The large activation energies indicate a reduced mobile carrier density as one reason for the decrease in conductivity upon Si anodization. With the same dopant concentration ($> 10^{18}\,\mathrm{cm}^{-3}$) in bSi and pSi, complete ionization of dopant atoms in bSi and only accounting for the exponential term in Equation (1), one estimates for a sample with $E_A^\sigma = 400$meV at 600K ($\rightarrow k_B T \approx 52$meV) a reduction in free carriers by $\exp(-400/50) \approx 5 \times 10^{-4}$ compared to bSi.

Deducing the origin of the intersample variation in E_A^σ is an intriguing task as all samples are anodized bona fide under the same electrochemical conditions. The anodization of different pSi samples is considered reproducible with respect to average pore size $\overline{R}$ and porosity ϕ. Marginal sample-to-sample variations in $\overline{R}$ and ϕ can be neglected and exhibit most importantly no systematic correlation with activation energy E_A^σ variations. It is therefore imperative to conclude that the parameters porosity ϕ and average pore size $\overline{R}$ are not sufficient to uniquely characterize the microstructure that determines the electrical properties.

The picture of an ensemble of different, possible microstructural configurations for the two macroscopic variables $\overline{R}$ and ϕ emerges in which the ensemble averages for transport quantities do not agree with the inherently provided volume averages of the transport measurements. Borrowing an expression from statistical mechanics, the samples exhibit a lack of ergodicity, which finally allows to determine the transport mechanism in pSi as put forward in the remainder of this article.

The Arrhenius plot of the thermally activated conductivities (Figure 1) exhibits one attention seeking peculiarity. Irrespective of the sample and its activation energy, all datasets and their nonlinear least squares approximations intersect within a reasonable margin of error in one single point at a characteristic temperature T_{MN}. This is a manifestation of a so-called Meyer–Neldel compensation rule (MNR) that implies an intersample relation between the quantities σ_0 and E_A^σ. It is

$$\sigma_0 = \sigma_{00} \exp\left(E_A^\sigma \Big/ E_{MN}\right) \tag{2}$$

with the Meyer–Neldel energy $E_{MN} = k_B T_{MN}$.

Figure 3 shows the nonlinear squares approximation of this intersample correlation based on Equation (2). As a Meyer–Neldel energy, one finds $E_{MN} \approx 58$meV. Surprisingly, this energy value is close to a prominent, sharp maximum in the optical phonon density-of-states of silicon.[47] It is therefore tempting to focus attention solely on phonon-assisted hopping models in an attempt to answer the stated key question concerning the charge carrier transport. However, this agreement is deceptive and no more than coincidental as argued below.

The Meyer–Neldel rule in pSi finds an explanation on fundamental grounds as direct manifestation of the microscopic mechanisms that govern carrier transport in this porous, disordered material. Key statements of the novel MNR model put forward by this article concern the band structure of pSi: 1) a mobility edge E_C separates extended Bloch states from localized Anderson states;[48,49] 2) it is $E_C > E_F$ and only charge carriers above the mobility edge in extended states contribute to charge transport; 3) interfaces and defects cause midgap states;[50] 4) the Fermi-level E_F is pinned in the center of the bandgap in the energy range of the midgap states;[50,51] 5) the mobility edge is located in the band tail with an exponential density-of-states

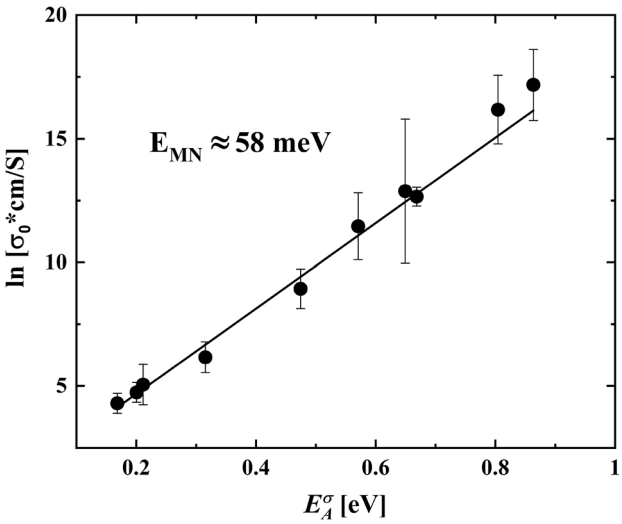

Figure 3. Meyer–Neldel compensation rule for pSi. The solid line is a nonlinear least squares approximation according to Equation (2). Note: different data points correspond to different samples.

$N(E)$; and finally, 6) E_C depends strongly on the degree of microscopic disorder.[42,52]

The model is conceived so far and subsequently for the more familiar case of electron transport. Adapting to hole transport is obviously trivial. With statements #1 and #2, one writes directly for the electrical conductivity in the Drude model

$$\sigma = \underbrace{eN(E_C)\mu(T)k_B T}_{\sigma_0} \exp\left(-\frac{E_C - E_F}{k_B T}\right) \tag{3}$$

Here, $\mu(T)$ is a temperature-dependent carrier mobility that is dominated by carrier scattering on the disordered nanostructure in pSi. In ansatz Equation (3), only charge carriers in the energy interval $[E_C, E_C + k_B T]$ contribute significantly to the charge transport. However, the total temperature dependence of σ_0 is negligible in the same spirit as in Equation (1), which is the basis of the original data analysis.

Statements #3 and #4 are motivated by insights from studies on disordered, amorphous semiconductors.[42,50,51] Essentially, statements #5 and #6 explain the MNR as a direct consequence of the exponential density of states in a band tail $N(E_C) \propto \exp(E_C/E_{MN})$ and an intersample variation of E_C. $E_C - E_F$ is identified as activation energy E_A^σ.

It remains statement #6 for additional discussion. One assumes different microstructural configurations to be realized in different samples (see above) that manifest in a varying degree of disorder. It is this disorder that has an significant impact on the position of the mobility edge E_C. A quantitative, theoretical description of this effect is challenging. It strongly depends on the system under discussion and requires a microscopic model for disorder. Abou-Chacra and Thouless,[52] for instance, showed that the position of the mobility edge in a simple Anderson model[53] varies with the mean square deviation of the site energy in the limit of low disorder.

The novel explanation of the MNR in pSi appeals through simplicity and elegance. However, the observation of phenomenological compensation rules is well documented for diverse transport processes and MNRs for thermally activated electrical conductivity, atomic diffusion, or thermal emission of charge carriers were intensively studied in contemporary scientific literature before.[6,54–67] Consequently, a brief review of the two most prominent but entirely different explanation attempts for compensation rules is in order.

Lubianiker and Balberg[60] reported in 1997 an MNR for the DC conductivity in pSi. By drawing parallels with the behavior of amorphous silicon, they infer an extended-state transport mechanism in pSi. As of the origin of the MNR, the authors remain fairly vague but vote for a level-shift model in which the chemical potential E_F depends linearly on temperature T. This fairly conveniently chosen temperature dependence, however, requires an asymmetric, particularly tailored density-of-states around E_F.[59]

In Yelon's[64] multiexcitation entropy (MEE) model, charge transport is considered as a thermodynamic activation process with rate $X \propto \exp(-\Delta G/k_B T)$ utilizing the Gibbs free energy G as appropriate thermodynamic potential. With the fundamental relation between the Gibbs free energy G, the enthalpy H and entropy S of the system it is $X \propto \exp(\Delta S/k_B) \times \exp(-\Delta H/k_B T)$ and the derivation of the MNR is complete with $E_A = \Delta H$ if $\Delta S/k_B = \Delta H/E_{MN}$.

The entire reasoning relies on the intuitive argument that a large number of phonons (excitations) must be absorbed in a thermal fluctuation to overcome an activation barrier, which is much larger than the thermal energy $k_B T$ and the phonon energy itself. This absorption process comes along with a large "selection" entropy ΔS as there are multiple ways how to absorb the required number of phonons. It is this entropy that increases with the activation energy and causes the compensation factor.[64–66] In particular, E_{MN} relates directly to the energy spectrum of the phonons.

Although passionately challenged by Fishchuk et al.[57] Yelon et al.[64] draw confidence in their theory from the microscopic, optical-phonon-assisted charge-hopping models developed by Emin.[46] In an impressively extended and convoluted calculation, Emin derives the multiphonon-assisted hopping rate for a two-site model, which includes a compensation factor and allows assigning a Meyer–Neldel energy via

$$E_{MN} = \frac{\hbar\omega_0}{\ln(M)}, \qquad M = \frac{2M_{eph}}{\hbar\omega_0} \tag{4}$$

Here, $\hbar\omega_0$ is a dispersionless optical phonon energy and M_{eph} is the electron–phonon coupling strength.

In the MEE framework, it is tempting to explain the MNR in pSi by multiphonon absorption enabled, thermally activated carrier hopping in localized states because of the exceptional agreement between E_{MN} and the maximum in the phonon density-of-states of Si/pSi. Yielding to this temptation is, however, premature and causes an unfortunate case of circular logic. The current state of the MEE theory only predicts a proportionality between E_{MN} and the energy of the phonons, a proportionality whose details depend on the microscopic model. For instance, in Equation (4), one has to assume ad hoc an electron–phonon coupling parameter $M_{eph} \approx 78$meV to obtain $E_{MN} = \hbar\omega_0 = 58$meV. This coupling constant might not be unreasonable by any scientific grounds but appears to be arbitrarily chosen with the sole purpose to recover the identity between the Meyer–Neldel energy and the maximum in the phonon density-of-states, an identity which motivates the application of the MEE theory on pSi in the first place.

Invaluable insight comes from temperature-dependent thermopower measurements $S(T)$ in **Figure 4** to resolve the issue of a charge carrier transport that is either governed by extended or localized states even more stringently. Therefore, data are compared with least-squares approximations based on the theoretical predictions for the thermopower of nondegenerate or amorphous semiconductors:[42]

$$S(T) = \frac{k_B}{e}\left(\frac{E_A^S}{k_B T} + A\right) \tag{5}$$

E_A^S refers to a characteristic activation energy for the carrier transport and A encodes details of the scattering mechanisms.[68]

The positive sign of the thermopower evidences hole transport in pSi. For bSi, a value $E_A^S = 45$meV is found in excellent agreement with the energy of the boron donor level in the Si bandgap.[41] The comparison of the experimentally observed

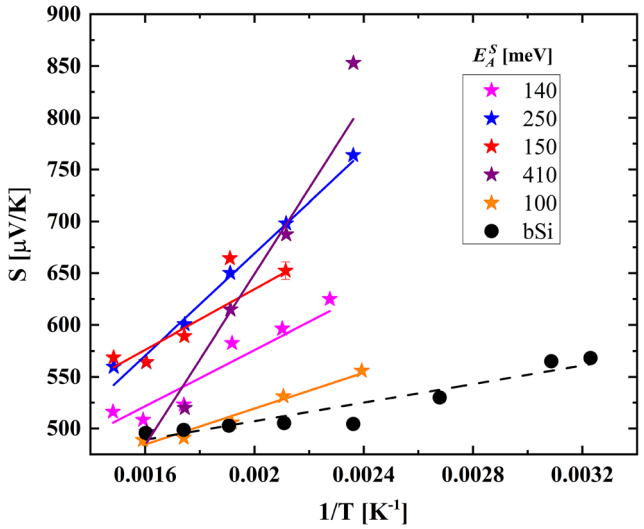

Figure 4. Thermopower of selected pSi samples as function of temperature. For clarity, only a representative subset of the data in Table 1 is shown. The solid lines are least-squares approximations based on Equation (5). The color and symbol code corresponds to the one of Figure 1. Error bars are of a similar size than the symbols. The black symbols refer to bulk Si.

activation energy for the conductivity and for the thermopower demonstrates the strict inequality $E_A^\sigma > E_A^S$ (**Table 1**) to hold for the entire ensemble of samples investigated. This seemingly trivial observation has important implications for the transport mechanism in pSi.

In crystalline materials, one expects the identity $E_A^\sigma \equiv E_A^S$ for charge transport in extended states.[42] Random potentials cause a pronounced inequality between both quantities for extended-state transport in disordered systems[42,69] such as amorphous silicon.[70] For hopping transport in localized states, $E_A^\sigma > E_A^S$ applies.[42] The hopping manifests in an exponential temperature dependence $\exp(-E_{hop}/k_B T)$ of the mobility accounting for the necessity to absorb phonons and it becomes elementary to show in Boltzmann transport theory that $E_{hop} = E_A^\sigma - E_A^S$.[43]

It is finally the inequality between E_A^σ and E_A^S why an explanation of the MNR in pSi based on MEE models fails. Assuming a hopping mechanism combined with the thermopower results requires discussing the MNR in terms of E_{hop} and not E_A^σ. But Table 1 clearly shows that there is no MNR observed for E_{hop} that relates, in this scenario, to the energy barrier between hopping sites and thus would define the number of phonons that must be absorbed to accomplish intersite jumps.

3. Conclusion

The electronic transport in doped, crystalline silicon is well understood. In the extrinsic temperature region,[41] the doping level defines the temperature independent charge carrier concentration in extended Bloch states of the conduction band. Upon carrier flow, it is the scattering on phonons and impurities that determines the temperature dependence of the conductivity.

This article refines this picture for pSi. Porosification causes disorder-induced, localized Anderson states in the band tails, gap states, and charge carrier depletion accompanied by band bending at the huge internal interfaces. The bandgap in pSi is significantly increased compared to bSi. The electrical conductivity in pSi is thermally activated. It is controlled by the temperature-dependent carrier concentration rather than the different scattering mechanisms. Activation energies reach values up to 860meV.

Electrical conductivity measurements reveal a Meyer–Neldel compensation rule for the thermally activated transport. A novel explanation for the MNR bases on Fermi-level pinning in midgap states, exponential density-of-states in the band tails, and transport in extended states above a disorder-dependent mobility edge. Thermopower measurements dispel the alternative hypothesis that multiphonon-assisted hopping in localized states causes the MNR in pSi.

The study provides novel and unique insights into the microscopic carrier transport mechanisms in pSi. As such, it is of interest to both fundamental science and applied science. In particular, material scientists who seek to develop pSi/nanostructured Si-based energy materials, e.g., supercapacitors or thermoelectrics will benefit from these findings.

4. Experimental Section

Sample Synthesis: The synthesis of pSi is achieved through the anodization of single-crystalline, p-doped silicon wafers in electrolytes containing HF acid.[33–35,71] The most critical control parameters of the anodization process are the HF concentration, current density, and etching time. With the appropriate resistivity and crystallographic orientation of the silicon wafers used, it is possible to control pore sizes, porosity, and interconnectivity of the etched pore networks.

The samples for the present study are synthesized by electrochemical etching of p-type [001]-oriented silicon wafers with a conductivity of $\sigma = 50 - 100\,\mathrm{S\,cm^{-1}}$. The wafers are anodized in a 4:6 electrolyte solution comprising 48 vol% HF and 99 vol% ethanol, with an etching current density of $j = 12\,\mathrm{mA\,cm^{-2}}$. Following a 4 hour etching process, an increased current density of $j = 216\,\mathrm{mA\,cm^{-2}}$ is applied for 40s to detach 160 µm thick, self-supporting membranes with a diameter of roughly 5 cm from the bulk wafers.

Sample Characterization: The etched pSi membranes are characterized by nitrogen N_2 sorption isotherms, which provide information about the morphological properties of the samples. The analysis of isotherms

Table 1. Activation energies for electrical conductivity and thermopower.

pSi sample	#1	#2	#3	#4	#5	#6	#7	#8	#9	#10
E_A^σ [meV]	863 ± 58	668 ± 14	474 ± 32	571 ± 62	804 ± 57	650 ± 135	315 ± 123	200 ± 16	212 ± 35	168 ± 15
E_A^S [meV]	460 ± 92	150 ± 65	100 ± 57	250 ± 16	410 ± 52	100 ± 77	140 ± 34	100 ± 10	100 ± 26	100 ± 11
$E_A^\sigma - E_A^S$ [meV]	403 ± 109	518 ± 66	374 ± 65	321 ± 64	394 ± 77	550 ± 155	175 ± 41	100 ± 19	112 ± 44	68 ± 19

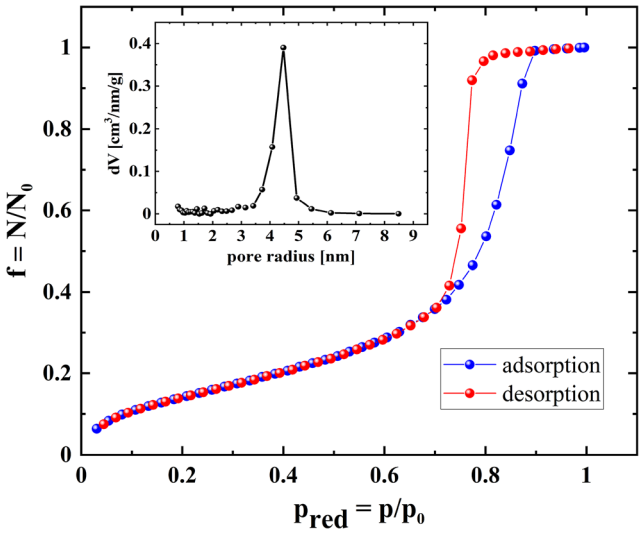

Figure 5. Nitrogen sorption isotherm of pSi measured at $T = 77$K. The inset shows the pore size distribution as obtained from the Barrett–Joyner–Halenda analysis.

guarantees that only morphologically identical samples are selected for subsequent charge transport measurements.

Figure 5 shows a representative N_2 sorption isotherm of a single membrane at $T = 77$K. The nanoscale properties of the pSi sample determine the volumetric liquid- N_2 uptake $f = N/N_0$ upon increasing or decreasing the partial vapor pressure $P_{red} = P/P_0$. N and N_0 are the number of physisorbed N_2 molecules at partial and complete pore filling whereas P and P_0 refer to the N_2 vapor pressure below and at saturation ($P_0(77\text{K}) = 1013$mbar).

A Barrett–Joyner–Halenda analysis[72] of the desorption measurements identifies an average pore radius of $\overline{R} = 4.5$ nm for the mesoporous membranes. A specific surface of $A \approx 160\,\text{m}^2\text{g}^{-1}$ is inferred from a Brunauer–Emmet–Teller analysis[73] of the low-pressure part of the isotherm prior to the onset of capillary condensation. Finally, the membrane volume and N_0 allow for the estimation of the porosity to be $\phi \approx 55\%$.

Charge-Transport Measurements: Electrical conductivity and thermopower of freestanding pSi membranes are measured with a commercial Seebeck Analyzer (SBA 458 Nemesis, NETZSCH-Gerätebau GmbH, Germany) in the temperature range from 300 to 673K. A nitrogen gas atmosphere prevents sample oxidation at elevated temperatures. Transport properties are probed in-plane of the roughly 10 mm long, rectangular-shaped samples.

An in-line four-point probe technique (current injection: rhodium tips; voltage measurement: Inconel-covered type K thermocouples) is used to determine the electrical conductivity at a maximum current of 1 mA. The thermopower is determined from the voltage drop across the two thermocouples in response to an applied temperature gradient $\Delta T < 7.5$K.

Acknowledgements

The authors thank the research school MatSec for project support. The authors thank the DFG for funding the project "Hybrid thermoelectrics based on porous silicon: Linking Macroscopic Transport Phenomena to Microscopic Structure and Elementary Excitations," project number 402553194.

Conflict of Interest

The authors declare no conflict of interest.

Author Contributions

Tommy Hofmann: conceptualization (lead); formal analysis (lead); funding acquisition (lead); supervision (lead); writing—original draft (lead). **Haider Haseeb**: data curation (lead); investigation (lead). **Danny Kojda**: investigation (supporting); resources (lead). **Natalia Gostkowska-Lekner**: investigation (supporting). **Klaus Habicht**: supervision (lead); writing—review and editing (lead).

Data Availability Statement

The data that support the findings of this study are available from the corresponding author upon reasonable request.

Keywords

disorder, localization, mobility edge, nanostructure, silicon

Received: August 15, 2024
Revised: January 20, 2025
Published online:

[1] M. Amato, S. Ossicini, E. Canadell, R. Rurali, *Nano Lett.* **2019**, *19*, 866.
[2] L. Bu, S. Guo, X. Zhang, X. Shen, D. Su, G. Lu, X. Zhu, J. Yao, J. Guo, X. Huang, *Nat. Commun.* **2016**, *7*, 11850.
[3] F. Márquez, C. Morant, V. López, F. Zamora, T. Campo, E. Elizalde, *J. Phys. Chem. C* **2011**, *6*, 495.
[4] S. Sun, F. Jaouen, J.-P. Dodelet, *Adv. Mater.* **2008**, *20*, 3900.
[5] J. H. Olshansky, A. D. Balan, T. X. Ding, X. Fu, Y. V. Lee, A. P. Alivisatos, *ACS Nano* **2017**, *11*, 8346.
[6] A. I. Yakimov, A. V. Dvurechenskii, A. I. Nikiforov, G. Y. Mikhalev, *J. Exp. Theor. Phys. Lett.* **2004**, *80*, 321.
[7] T. Hofmann, E. Dobisz, B. M. Ocko, *J. Vac. Sci. Technol. B* **2009**, *27*(6), 3238.
[8] T. Hofmann, M. Tasinkevych, A. Checco, E. Dobisz, S. Dietrich, B. M. Ocko, *Phys. Rev. Lett.* **2010**, *104*, 106102.
[9] S. Cataldo, B. Pignataro, *Materials* **2013**, *6*, 1159.
[10] U. Lang, E. Müller, N. Naujoks, J. Dual, *Adv. Funct. Mater.* **2009**, *19*, 1215.
[11] D. P. Sellan, J. E. Turney, A. J. H. McGaughey, C. H. Amon, *J. Appl. Phys.* **2010**, *108*, 113524.
[12] J. E. Allen, K. G. Yager, H. Hlaing, C.-Y. Nam, B. M. Ocko, C. T. Black, *Appl. Phys. Lett.* **2011**, *99*, 163301.
[13] B. Bouthinon, R. Clerc, J. Vaillant, J.-M. Verilhac, J. Faure-Vincent, D. Djurado, I. Ionica, G. Man, A. Gras, G. Pananakakis, R. Gwoziecki, A. Kahn, *Adv. Funct. Mater.* **2015**, *25*, 1090.
[14] B. A. Rahim, B. Abderraouf, K. Gitanjali, R. Andreas, A. Richard, *Small* **2017**, *13*, 1603269.
[15] U. Treske, N. Heming, M. Knupfer, B. Büchner, E. Di Gennaro, A. Khare, U. S. Di Uccio, F. M. Granozio, S. Krause, A. Koitzsch, *Sci. Rep.* **2015**, *5*, 14506.
[16] H. Wu, J. Yang, S. Cao, L. Huang, L. Chen, *Macromol. Chem. Phys.* **2014**, *215*, 584.
[17] P. Huber, *J. Phys.: Condens. Matter* **2015**, *27*, 103102.
[18] D. Kojda, D. Wallacher, S. Baudoin, T. Hansen, P. Huber, T. Hofmann, *J. Chem. Phys.* **2014**, *140*, 024705.
[19] K. Sentker, A. W. Zantop, M. Lippmann, T. Hofmann, O. H. Seeck, A. V. Kityk, A. Yildirim, A. Schönhals, M. G. Mazza, P. Huber, *Phys. Rev. Lett.* **2018**, *120*, 067801.
[20] D. Wallacher, T. Hofmann, K. Knorr, A. V. Kityk, *Phys. Rev. B* **2005**, *71*, 224202.

[21] C. Dames, G. Chen, *J. Appl. Phys.* **2003**, *95*, 682.
[22] D. Li, Y. Wu, P. Kim, L. Shi, P. Yang, A. Majumdar, *Appl. Phys. Lett.* **2003**, *83*, 2934.
[23] N. Mingo, L. Yang, D. Li, A. Majumdar, *Nano Lett.* **2003**, *3*, 1713.
[24] P. G. Murphy, J. E. Moore, *Phys. Rev. B* **2007**, *76*, 155313.
[25] P. E. Hopkins, L. M. Phinney, P. T. Rakich, R. H. Olsson, I. El-Kady, *Appl. Phys. A* **2010**, *103*, 575.
[26] T. Hofmann, D. Wallacher, R. Toft-Petersen, B. Ryll, M. Reehuis, K. Habicht, *Microporous Mesoporous Mater.* **2017**, *243*, 263.
[27] T. Hofmann, D. Kojda, H. Haseeb, D. Wallacher, O. Sobolev, K. Habicht, *Microporous Mesoporous Mater.* **2021**, *312*, 110814.
[28] D. Kojda, T. Hofmann, N. Gostkowska-Lekner, K. Habicht, *Nano Res.* **2022**, *15*, 5663.
[29] Y. Xue, J. Markmann, H. Duan, J. Weissmüller, P. Huber, *Nat. Commun.* **2014**, *5*, 4237.
[30] M. Busch, T. Hofmann, B. Frick, J. P. Embs, B. Dyatkin, P. Huber, *Phys. Rev. Mater.* **2020**, *4*, 055401.
[31] T. Hofmann, D. Wallacher, M. Mayorova, R. Zorn, B. Frick, P. Huber, *J. Chem. Phys.* **2012**, *136*, 124505.
[32] T. Hofmann, in *Nanostructured Energy Materials: From Organic Photovoltaic to Hybrid Thermoelectrics*, World Scientific, Singapore **2020**, pp. 435–479.
[33] L. Canham, in *Handbook of Porous Silicon*, Springer International Publishing, Cham, Switzerland **2014**.
[34] M. J. Sailor, in *Porous Silicon in Practice: Preparation, Characterization and Applications*, Wiley-VCH, Weinheim, Germany **2012**.
[35] X. G. Zhang, *J. Electrochem. Soc.* **2004**, *151*, C69.
[36] E. J. Anglin, L. Cheng, W. R. Freeman, M. J. Sailor, *Adv. Drug Delivery Rev.* **2008**, *60*, 1266.
[37] W. Li, Z. Liu, F. Fontana, Y. Ding, D. Liu, J. T. Hirvonen, H. A. Santos, *Adv. Mater.* **2018**, *30*, 1703740.
[38] H. Jia, X. Li, J. Song, X. Zhang, L. Luo, Y. He, B. Li, Y. Cai, S. Hu, X. Xiao, C. Wang, K. M. Rosso, R. Yi, R. Patel, J.-G. Zhang, *Nat. Commun.* **2020**, *11*, 1474.
[39] L. Oakes, A. Westover, J. W. Mares, S. Chatterjee, W. R. Erwin, R. Bardhan, S. M. Weiss, C. L. Pint, *Sci. Rep.* **2013**, *3*, 3020.
[40] G. Romano, A. Di Carlo, J. C. Grossman, *J. Comput. Electron.* **2012**, *11*, 8.
[41] S. M. Sze, in *Semiconductor Devices: Physics and Technology*, John Wiley & Sons, Singapore **2012**.
[42] N. F. Mott, E. A. Davis, in *Electronic Processes in Non-crystalline Materials*, OUP, Oxford **2012**.
[43] G. Czycholl, Theoretische Festkörperphysik: Von den klassischen Modellen zu modernen Forschungsthemen, Springer, Berlin Heidelberg **2007**.
[44] V. Sa-Yakanit, H. R. Glyde, Comments on Condensed Matter Physics, Gordon & Breach, New York **1987**.
[45] A. L. Efros, B. I. Shklovskii, *J. Phys. C: Solid State Phys.* **1975**, *8*, L49.
[46] D. Emin, *Adv. Phys.* **1975**, *24*, 305.
[47] D. S. Kim, H. L. Smith, J. L. Niedziela, C. W. Li, D. L. Abernathy, B. Fultz, *Phys. Rev. B* **2015**, *91*, 014307.
[48] S. Janßen, J. Mesot, L. Holitzner, A. Furrer, R. Hempelmann, *Phys. B: Condens. Matter* **1997**, *234–236*, 1174.
[49] N. Mott, *J. Phys. C: Solid State Phys.* **1987**, *20*, 3075.
[50] N. F. Mott, *J. Phys. C: Solid State Phys.* **1980**, *13*, 5433.
[51] E. A. Davis, N. F. Mott, *Philos. Mag.* **1970**, *22*, 0903.
[52] R. Abou-Chacra, D. J. Thouless, *J. Phys. C: Solid State Phys.* **1974**, *7*, 65.
[53] P. W. Anderson, *Phys. Rev.* **1958**, *109*, 1492.
[54] A. Dalvi, N. P. Reddy, S. C. Agarwal, *Solid State Commun.* **2012**, *152*, 612.
[55] T. Drüsedau, D. Wegener, R. Bindemann, *Phys. Status Solidi B* **1987**, *140*, K27.
[56] I. I. Fishchuk, A. Kadashchuk, A. Mityashin, M. M. Gavrilyuk, A. Köhler, H. Bässler, J. Genoe, H. Sitter, N. S. Sariciftci, *Phys. Rev. B* **2014**, *90*, 245201.
[57] I. I. Fishchuk, H. Bässler, A. Köhler, J. Genoe, A. Kadashchuk, *Phys. Rev. Appl.* **2018**, *10*, 054063.
[58] A. Juma, H. Wafula, E. Wendler, T. Dittrich, *J. Appl. Phys.* **2014**, *115*, 053703.
[59] M. Kikuchi, *J. Appl. Phys.* **1988**, *64*, 4997.
[60] Y. Lubianiker, I. Balberg, *Phys. Rev. Lett.* **1997**, *78*, 2433.
[61] R. Metselaar, G. Oversluizen, *J. Solid State Chem.* **1984**, *55*, 320.
[62] G. Oversluizen, R. P. van Kessel, K. J. Nieuwesteeg, J. Boogaard, *J. Appl. Phys.* **1991**, *69*, 3082.
[63] R. Widenhorn, A. Rest, E. Bodegom, *J. Appl. Phys.* **2002**, *91*, 6524.
[64] A. Yelon, B. Movaghar, R. S. Crandall, *Rep. Prog. Phys.* **2006**, *69*, 1145.
[65] A. Yelon, B. Movaghar, H. M. Branz, *Phys. Rev. B* **1992**, *46*, 12244.
[66] A. Yelon, B. Movaghar, *Phys. Rev. Lett.* **1990**, *65*, 618.
[67] P. T. Landsberg, in *Handbook on Semiconductors*, Elsevier Science **2016**.
[68] M. Lundstrom, in *Fundamentals of Carrier Transport*, Cambridge University Press, New York **2009**.
[69] H. Overhof, *Phys. Status Solidi B* **1975**, *67*, 709.
[70] H. M. Dyalsingh, J. Kakalios, *Phys. Rev. B* **1996**, *54*, 7630.
[71] N. Gostkowska-Lekner, D. Wallacher, N. Grimm, K. Habicht, T. Hofmann, *Rev. Sci. Instrum.* **2020**, *91*, 105113.
[72] E. P. Barrett, L. G. Joyner, P. P. Halenda, *J. Am. Chem. Soc.* **1951**, *73*, 373.
[73] S. Brunauer, P. H. Emmett, E. Teller, *J. Am. Chem. Soc.* **1938**, *60*, 309.
[74] J. Tauc, *Mater. Res. Bull.* **1968**, *3*, 37.
[75] C.-Y. Tsai, *J. Appl. Phys.* **2018**, *123*, 183103.